Synthesis and Properties of Highly Dispersed Ionic Silica–Poly(ethylene oxide) Nanohybrids

Nikhil J. Fernandes,[†] Johanna Akbarzadeh,[‡] Herwig Peterlik,[‡] and Emmanuel P. Giannelis[§,*]

[†]School of Applied and Engineering Physics and [§]Department of Materials Science and Engineering, Cornell University, Ithaca, New York 14853, United States and [‡]Faculty of Physics, University of Vienna, Strudlhofgasse 4, A-1090 Vienna, Austria

ABSTRACT We report an ionic hybrid based on silica nanoparticles as the anion and amine-terminated poly(ethylene oxide) (PEO) as a cation. The charge on the nanoparticle anion is carried by the surface hydroxyls. SAXS and TEM reveal an exceptional degree of dispersion of the silica in the polymer and high degree of order in both thin film and bulk forms. In addition to better dispersion, the ionic hybrid shows improved flow characteristics compared to silica/PEO mixtures in which the ionic interactions are absent.

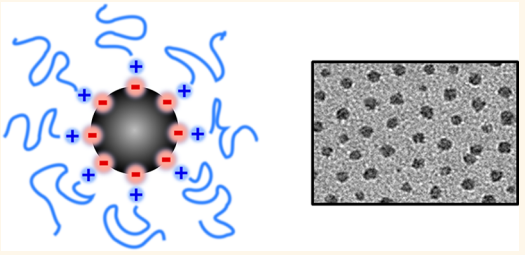

KEYWORDS: nanoscale ionic materials · nanoparticle dispersion · nanohybrids · core–shell hybrids · self-assembled hybrids

One of the major challenges at the forefront of research into nanoparticle/polymer systems is nanoparticle dispersion. The spatial distribution of nanoparticles in the polymer matrix affects a range of properties, from flow and strength to electrical and thermal conductivity. More control over nanoparticle dispersion could allow better property "tuning" and provide appropriate functionality.[1−4] In particular, the ability to keep nanoparticles isolated and uniformly dispersed is critical in creating hybrid materials that retain the fluidity of the host polymer while incorporating a high fraction of inorganic particles with their associated properties.[1,5] Fluids with high nanoparticle content are of particular interest for applications such as lubricants,[6,7] high refractive index materials for lithography,[8] battery electrolytes,[9] carbon capture materials,[10] and other applications where processability demands fluidity but functionality demands a high inorganic content. However, dispersing nanoparticles uniformly in a polymer is often challenging. Flory–Huggins theory suggests that in order to achieve a stable and uniform dispersion, the particle and polymer have to be chemically compatible, that is, with an interaction parameter $\chi \leq 0$.[2] This is achieved in one of two ways; either by choosing an appropriate nanoparticle/polymer combination (such as cross-linked polystyrene particles and a linear polystyrene host), or by grafting short oligomeric or polymeric chains to the surface of the particle, creating a "corona" that has a favorable interaction parameter with the host.[11−14] The first approach limits the choice of materials in the composite. Additionally, it has been shown by Mackay *et al.* that this approach is limited to systems where the radius of the particle is less than the radius of gyration (R_g) of the polymer.[2] The second approach is more general, with a vast library of core/shell particle systems that have been made by a variety of methods,[15] but the dispersion characteristics are highly sensitive to the graft density and molecular weight of the corona and host matrix.[16] The sensitivity of the final structure to precise synthetic control of the materials, in addition to the chemistry required to graft the corona or grow it from the surface of the particle, imposes limits on scale-up and commercial production.

An alternative approach is to graft short oligomeric chains with ionic functionalities to the particles, and then react those functionalities with a polymer end-terminated with a functionality of the opposite charge.[17−26] These nanoparticle ionic materials (NIMs) are notable because they are more similar to one-phase, solvent-free molten salts than

* Address correspondence to epg2@cornell.edu.

Received for review October 12, 2012 and accepted January 25, 2013.

Published online January 27, 2013
10.1021/nn304735r

two-phase dispersions of nanoparticles. While NIMs have been demonstrated with several nanoparticle cores as diverse as metal oxides,[21,22,26,27] chalcogenides,[20] and metals,[19] all these systems still require the modification of the nanoparticle surface with a molecular corona to impart the necessary charge. For example, in silica-based NIMs the nanoparticles are typically reacted with a silane comprising a terminal sulfonic acid or amine group.[23] While this approach has the advantage of producing a more tunable platform, it does not eliminate the grafting and purification steps entirely.

We describe here an alternative system where we exploit the favorable interactions between the polymer and the nanoparticles using an end-functionalized amine-terminated polymer (PEO-NH_2) to react with the inherently acidic hydroxyl groups present on the surface of silica (SiO_2) nanoparticles. We show that despite the relatively high inorganic content the SiO_2 nanoparticles are well dispersed due to the ionic interactions present in this system and the material behaves distinctly different from systems where these interactions are absent. First, the ionic hybrids show a high-degree of order in both thin film and bulk forms. Second, the unique dispersion of the nanoparticles endows them with a liquid-like character despite their high inorganic content. In contrast, the controls show solid-like character and a yield stress consistent with nanoparticle aggregation and poor dispersion levels.

While we demonstrate the approach using silica nanoparticles, the method is general and can be used with a variety of nanoparticles provided that they possess surface groups that can act as acids or bases and interact with polymers containing appropriate groups. The favorable χ parameter due to the presence of strong ionic interactions ensures thorough mixing and an excellent dispersion of the nanoparticles within the polymer matrix. Either end-functionalized polymers or polymers with appropriate side groups can be utilized although the presence of multiple interaction sites could lead to cross-linked systems. We note that our approach uses commercially available colloidal silica making the process simple and scalable. In an earlier publication we focused on polyhydroxylated fullerenes,[25] but the small, well-defined molecular weight of fullerenes makes that material closer to a molecular ionic liquid than a true nanoparticle hybrid material. This approach is analogous to the use of ionic blend compatibilizers in creating well-dispersed polymeric blends,[28] with the difference being that one of the components in the blend is an inorganic nanoparticle (which has been shown to lead to an additional entropic penalty that has to be overcome).[2]

RESULTS AND DISCUSSION

Using the monomer length l_0 of 0.37 nm, C_∞ = 5.6, and 44.05 g mol^{-1} for the repeat unit and molecular mass for PEO we estimate the radius of gyration for a 20 kDa coil in a Θ solvent (and therefore also in the melt) to be 7.6 nm.[29] The pH and zeta potential of the as obtained, Na^+-stabilized silica suspension (0.03 g/mL) are 11 and −30 mV, respectively. Passing the silica through a proton exchanged resin results in a suspension with a pH of about 3 and a zeta potential of −5 mV. The pH and zeta potential values indicate that nearly all surface groups are in the neutral, protonated form.[30,31]

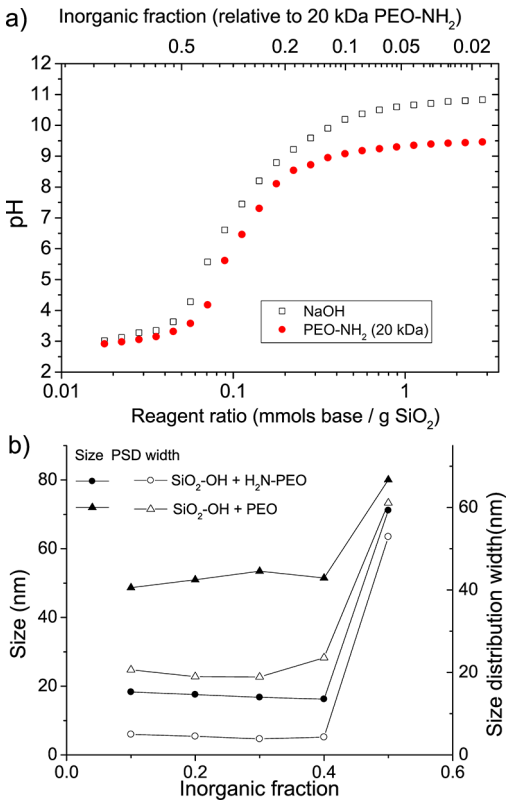

Figure 1. (a) pH *vs* reagent ratio for the reaction of the silica particles with 1.5 mM NaOH (open symbols) and 1.5 mM PEO-NH_2 (filled symbols). The upper axis shows the inorganic fraction for the ionic hybrid . (b) DLS results corresponding to the titration curves, showing modal size (filled) and size distribution width (open) for the ionic material (O) and a silica/PEO mixture (Δ).

The acidity of silica surface hydroxyls (silanols) is well established, although the exact pK_a values vary depending on the system. Typically, two pK_a values have been reported for silanols—one in the 4−5 range, and another in the 8−10 range.[32−34] The surface silanol density is about 4−5 −OH/nm^2, of which the more acidic groups are reported to be anywhere between 10% to 20%. We expect only the more acidic sites to take part in an acid−base reaction with PEO-NH_2

Figure 1a shows the pH profiles obtained in titrating NaOH solution and the amine-terminated polymer with the H^+-exchanged silica suspension. The reaction with PEO-NH_2 can be represented by

$$(SiO_2) - OH + H_2N - PEO \rightleftharpoons (SiO_2) - O^- H_3^+ N - PEO$$

As silica is added to the PEO-NH_2 solution the equilibrium shifts to the right and an ionic hybrid is formed. At a pH of 8.5, the zeta potential of the resulting suspension was about ζ = −17 mV, indicating that the protons

from the silanols have reacted with the terminal amine groups on the PEO, and the particles are again negatively charged. If more silica is added, the pH drops rapidly as the concentration of free acidic silanols increases. In contrast, when the $(SiO_2)-OH$ is added to PEG, the pH drops immediately to 4 as the number of free acidic silanol groups goes up from zero, and then remains essentially unchanged since there is nothing to counteract the acidity of the free silanols. The measured point of complete reaction as 0.28 mmol per gram of SiO_2 corresponds to an inorganic volume fraction of 0.15 in the hybrid with 20 kDa PEO-NH_2. If α is the inorganic mass fraction for a given hybrid, then the number of polymer molecules per particle N is given by

$$N = \frac{4}{3}\frac{\pi r^3 \rho_{core} N_A}{M_W}\left(\frac{1-\alpha}{\alpha}\right)$$

where ρ_{core} and r are the density and radius of the silica particle, N_A is Avogadro's number, and M_W is the molar mass of the polymer. If we take the equivalent point to be at $\alpha = 0.15$, we obtain $N = 805$ for the 20 kDa PEO, which corresponds to an active silanol density of 1 nm^{-2} and is in excellent agreement with the estimate of 20% of the total number of the silanol groups (5 OH/nm^2) being acidic.

Aliquots of the solution were taken at regular intervals during the titration experiment and the size was measured by dynamic light scattering. The particle size obtained is shown in Figure 1b. In the case of the amine-terminated PEO, the particles stay dispersed in solution until the pH drops below 6, at which point the solution becomes turbid and the particles aggregate, as seen by a jump in both the nominal particle size, and by the width of the size distribution.

The protonation of the silica and the formation of the ionic bonds are essential to obtaining a good dispersion of particles into the polymer. Figure 2a is a TEM micrograph of a sample consisting of 20% by weight SiO_2 nanoparticles and a 20 kDa PEO-NH_2, showing excellent dispersion with the silica nanoparticles evenly dispersed in the polymer. In contrast, aggregation and phase-separation of the particles in the polymer can be seen in Figure 2b, which shows a TEM micrograph of an identically prepared sample but where sodium-stabilized silica particles were used, and Figure 2c, which shows a TEM micrograph of an identically prepared sample with proton-exchanged silica particles and hydroxyl-terminated PEO.

PEO is known to absorb on the surface of silica *via* hydrogen-bonding involving terminal groups or the backbone ether oxygens.[35,36] In the case of the PEO-NH_2, the amine groups preferentially react with the surface silanols of the particles, and since there is a single reactive group per PEO-NH_2 molecule, each particle becomes surrounded with a layer of PEO-NH_2 chains. In contrast, with the PEO, the particles aggregate

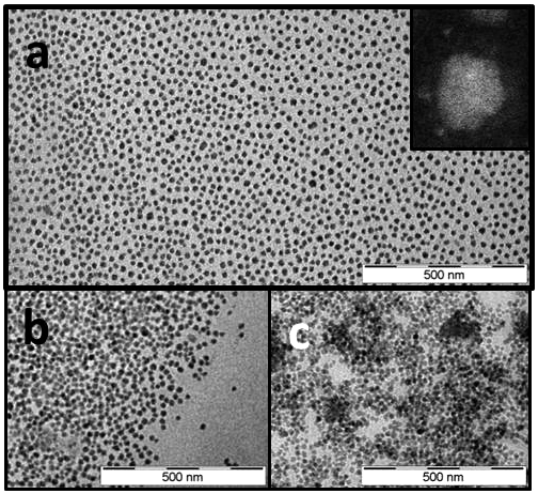

Figure 2. TEM images of (a) ionic material (with inset showing HAADF image of a single particle with a polymeric shell); (b) phase separated mixture of Na^+ stabilized particles mixed with polymer, and (c) HS30-OH particles mixed with unfunctionalized PEO.

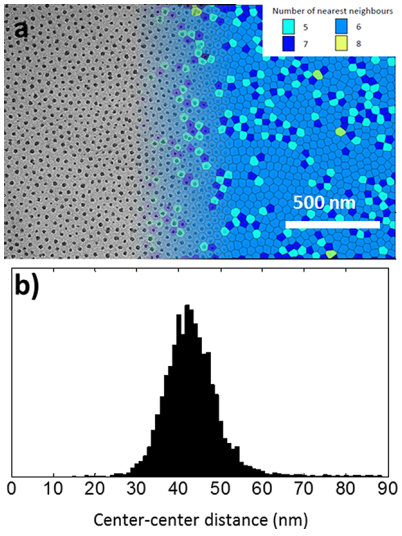

Figure 3. (a) Voronoi diagram of a TEM image of the ionic material, color-coded by coordination number of each cell. (b) Histogram of center-to-center distributions obtained from analyzing the Voronoi image.

immediately, even at low inorganic fractions, as seen in Figure 1b, a phenomenon that has been exploited to flocculate stable silica suspensions.

The "ordering" shown in Figure 2a can be analyzed to determine the packing geometry of the particles. The positions of the particle centers are extracted using the software package ImageJ, and then a Matlab script is used to create a Voronoi diagram. Figure 3a shows the same image with a superimposed Voronoi diagram. It is easy to see that the majority of particles are hexagonally coordinated, with "point defects" consisting of somewhat larger or smaller particles, and "line defects" consisting of alternating pentagonally and heptagonally coordinated particles. We conclude that the particles pack as spheres in 2D, which is consistent

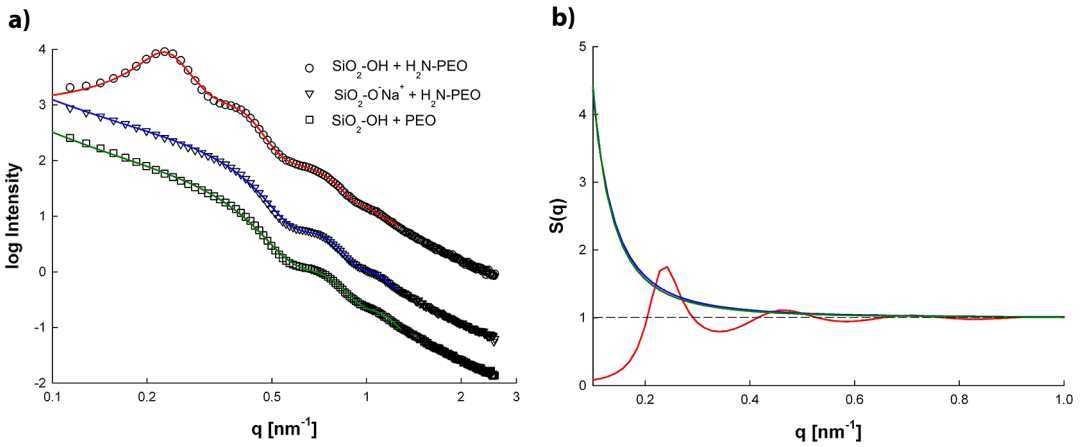

Figure 4. (a) Scattering curves of the ionic material (○), Na^+ stabilized HS30 particles in PEO (Δ) and HS30-OH mixed with unfunctionalized PEO (□). The curves are vertically shifted for better visibility. (b) Corresponding structure factors obtained from GIFT.

with a spherical shell surrounding each particle. This shell is invisible in brightfield TEM, but seen using HAADF-STEM (Figure 2a inset). The fact that the arrangement is not perfectly crystalline is due to inhomogeneity in the particle sizes. The defect lines in the Voronoi diagram do not form complete grain boundaries because the polymer shell is soft, allowing the defects to reabsorb into the hexagonal structure.

Small-angle X-ray scattering (SAXS) measurements were carried out on the ionic hybrid and both control samples in order to obtain structural information on the distribution of the particles. The samples were heated to 75 °C (above the melting temperature of PEO) to probe the arrangement of particles and eliminate any complications from the crystallinity of the PEO chains.

The scattering curves of all three samples are shown in Figure 4a. In general, the scattering intensity of a two-phase system of polydisperse particles can be described as the product of the form factor $P(q)$ and an effective structure factor $S(q)$ by $I(q) \propto (\Delta\rho)^2 P(q) S(q)$ where $\Delta\rho$ is the electron density difference between the two phases, that is, the silica core and the polymer matrix.[37]

For dilute systems with negligible interparticle interactions, the structure factor is constant, $S(q) = 1$. For such samples, the scattering curve can be fully described by the form factor $P(q)$.

All three samples show small modulations in the scattering intensity between $q = 0.4$ to 1.5 nm^{-1} which allows us to determine the amount of polydispersity and result in a mean diameter and a Gaussian half-width for silica particles with $d = 16 \pm 2$ nm, which is consistent with TEM measurements of the size of the particles. The ionic hybrid shows two additional peaks in the range between 0.2 and 0.4 nm^{-1}. They can be attributed to the short-range order, that is, the presence of electrostatic interactions between the negatively charged silica cores and the positively charged PEO-NH_2 chains, which leads to a regular arrangement with a characteristic particle-to-particle distance. From the position of the first peak, the distance between two silica particle centers is roughly $d = 2\pi/q_{max} = 27$ nm.

The control samples (Na^+ stabilized SiO_2 particles in PEO-NH_2 and SiO_2-OH mixed with unfunctionalized PEO) do not exhibit a distinct short-range order peak, but an intensity increase toward very low q-values. These results indicate some agglomeration and are described here by a structure factor from a fractal model.[38,39] To separate the effect from structure factor and form factor, we used the generalized indirect Fourier transformation (GIFT) for data evaluation.[40,41]

GIFT allows us to simultaneously determine both the pair distance distribution function $p(r)$ and pair correlation function $g(r)$, describing the shape of particles and their interaction in real space. Since the ionic material consists of charged particles, we decided to use the Yukawa potential for charged spheres as a structure factor model, which can be solved by a rescaled mean spherical approximation (RMSA).[42,43] From the model, one obtains a particle-to-particle distance of 27.2 nm from the first peak maximum of the structure factor (Figure 4b).[44] Additionally, one obtains an effective hard sphere volume fraction η, which describes the probability of finding two particles at a well-defined distance from each other, in analogy with the packing of hard spheres. The value of η is 0.38, suggesting a high degree of order in the system. Note that η in an ordered SC lattice is 0.52. The degree of ordering in the ionic hybrid system is even more astonishing considering that the measurements were carried out at 75 °C, where the system is a fluid.

In contrast, the structure factor in the control systems is described with a fractal model,[38,39] which corresponds to a wide range of different particle-to-particle distances. This agglomeration is also visible in the TEM images (Figure 2b and 2c). The wide size

distribution leads to no specific short-range order peak, but to an intensity increase toward low q-values (Figure 4a). The corresponding structure factors from the fractal model are shown in Figure 4b. The value for the fractal dimension is 2.4, indicating the mass fractal nature of the control samples. It should be noted that large agglomerates with a more well-defined size can be seen in Figure 2c, but their size is larger than 100 nm and a short-range order peak would not be within the accessible q-range of the SAXS measurements.

An estimate for the brush height of the polymer is given by[45]

$$\left(\frac{h}{H_0}\right)^3\left[1+\frac{3}{4}\left(\frac{h}{\omega H_0}\right)+\frac{1}{5}\left(\frac{h}{\omega H_0}\right)^2\right] = 1$$

where $H_0 = (8/\pi^2)^{1/3} l_0 n \nu^{1/3} \sigma^{*1/3}$, $\omega = (R_0/H_0)$, $\sigma^* = \sigma l_0^2$ and $\nu = ({}^1/_2 - \chi_{PP})$

With graft density $\sigma = 1$ nm^{-2}, degree of polymerization $n = 454$, nanoparticle radius $R_0 = 8$ nm, and setting the Flory parameter $\chi_{PP} = 0$ to capture the fact that in a melt the polymer is its own solvent, we can solve for h, obtaining $h = 21$ nm. If we consider each particle and its associated polymer as a single sphere, we would find (from the particle–particle separation of 27.2 nm calculated by SAXS) a brush height of 5.6 nm. The seemingly large discrepancy is explained by two factors. First, the polymers attached to neighboring particles interpenetrate strongly, since there is no other solvent in the system to swell the brushes. Second, there is a space-filling constraint; the polymer has to fill all the interstices between the hard spheres.[46] These two factors combine to reduce the particle–particle separation from the theoretically predicted value.

The larger particle–particle distance seen in the TEM images is believed to be a consequence of the drop-casting method for the preparation of thin samples: as the solvent evaporates, the core–shell spheres shrink anisotropically, forming disks that by conservation of volume have a larger lateral radius than the original sphere in 3 dimensions.

The consequences of a well-dispersed system of particles are dramatically manifested in their rheological behavior. Samples were characterized by imposing a constant oscillatory strain $\gamma(t) = \gamma_0 \sin(\omega t)$ within the linear viscoelastic regime, and monitoring the complex viscosity, $\eta^*(\omega)$, and the complex modulus, $G^*(\omega) = G' + iG''$. A convenient way to study different materials is to plot the complex viscosity as a function of the complex modulus (Figure 5).[47] The neat PEO-NH_2 behaves like a Newtonian fluid, with constant viscosity across the measured range of complex moduli. On the other hand, the controls, which show significant phase separation and aggregation by TEM and SAXS, show a divergent η^* at low G^*, characteristic of solid materials

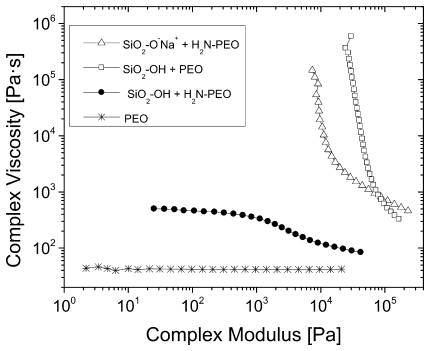

Figure 5. Cross plot of viscosity against complex modulus for Na+ stabilized particles in PEO (Δ), HS30-OH mixed with unfunctionalized PEO (□), the ionic material (●), and pure PEO (∗), showing that the ionic material is a viscoelastic fluid while the other materials are yielding solids.

with a yield stress. This divergence has been attributed to the formation of networks of particles within the material.[1,5] In contrast, the ionic hybrid shows shear thinning, but also has low viscosities across the entire span of complex moduli measured. We attribute this fluid-like behavior to three factors: First, the ability of the ionic hybrid to resist phase separation due to the more favorable polymer–particle interactions than polymer–polymer and particle–particle interactions, which prevents the formation of reinforcing particle networks. Second, the ability of chains to "hop" from one particle to another has been shown to enhance fluidity, as seen in NMR studies of other NIMs systems.[48] And finally, the outer portion of the polymer chains that occupies the interstices between the spheres acts as a solvent for the rest of the system.[49] The shear thinning behavior has been shown by simulations on solvent-free grafted polymer systems to be due to the alignment of chains in the material.[50]

CONCLUSIONS

We report a simple and scalable method of synthesizing well-dispersed nanoparticle/polymer hybrids comprising relatively high volume nanoparticle fractions by exploiting the electrostatic interactions as a result of an acid–base reaction between the native silanol groups of silica and an amine-terminated polymer. While we demonstrate here silica as a model system the approach can be easily extended to other oxide or nitride nanoparticles and polymers with complementary functional groups. The ionic hybrids show remarkable dispersion of the nanoparticles and appeared ordered in both thin films (TEM images) and bulk forms (SAXS). Control hybrid samples, where the ionic interactions have been turned off intentionally, show high levels of nanoparticle aggregation and behave more like conventional nanoparticle/polymer mixtures. The unique dispersion of the nanoparticles endows them with liquid-like character

despite their high inorganic content. In contrast, the controls show solid-like character and a yield stress consistent with nanoparticle aggregation and poor dispersion levels.

MATERIALS AND METHODS

Amine-terminated poly(ethylene oxide) (PEO-NH_2) (FW 20 kDa, PDI 1.02) was purchased from Laysan Biotech. Ludox sodium-stabilized, silica (HS30, average diameter 16 $\pm$ 2 nm), poly(ethylene oxide) (PEO) (FW 20 kDa) and Dowex HCR-W2 ion-exchange resin were obtained from Sigma Aldrich. All materials were used as supplied.

To create the ionic hybrid the HS30 silica suspension is first diluted to 3 wt % and passed three times through a column of H^+-exchanged Dowex resin to fully protonate the surface hydroxyls to form a suspension referred to as (HS30)$-$OH.

The optimal silica/PEO-NH_2 ratio was determined by first titrating a known volume of 3% (HS30)$-$OH solution with a 1.5 mM NaOH solution and monitoring the pH (Figure 1a). We find that the surface of the silica is neutralized (as evidenced by the change in the slope of the pH curve) at a ratio of 0.28 mmol of NaOH per gram of SiO_2 particles.

SiO_2/PEO-NH_2 hybrids were synthesized by adding the silica suspension dropwise to a 3% (1.5 mM) solution of PEG-NH_2 solution to reach the desired composition. The suspension was then stirred vigorously for about 6 h before it was frozen with liquid nitrogen and then placed in a lyophilizer to remove the water. All samples were then annealed at 75 °C in vacuum for 48 h before characterization.

Two control samples void of any ionic interactions were prepared for comparison following the procedure described above. In the first a hydroxyl-terminated poly(ethylene oxide) (MW 20 000) was used. In the second the pristine sodium-stabilized silica suspension (HS30)-Na^+ (without the H^+ exchange step) was added directly to the PEO-NH_2 solution.

For electron microscopy, the samples were diluted to 1% by weight in deionized water, and then a 5 μL drop was placed on a copper grid and allowed to rest for a minute before most of the water was blotted away. The grid was dried completely in air, and then annealed in vacuum at 75 °C before imaging. Bright-field TEM was carried out on a FEI Tecnai T12 microscope operating at 120 kV. High-angle annular dark field microscopy was carried out on a FEI Tecnai F20 microscope, operating at 200 kV. Dynamic light scattering and zeta potential measurements were carried out on a Malvern Instruments Zetasizer Nano. Rheological measurements were conducted on a Anton Paar MCR-501 rheometer with a peltier/nitrogen gas heating chamber and 25 mm diameter cone and plate geometry (measuring system CP25-1). All rheological measurements were carried out at 75 °C.

Small angle X-ray scattering (SAXS) experiments were carried out on a Bruker NanoStar Turbo X-ray source (rotating anode generator with CuKα radiation, wavelength 0.1542 nm) and equipped with a pinhole camera. The radiation is monochromatized and collimated with crossed Goebel mirrors. The samples were placed into quartz glass capillaries with 10 μm thick walls (Hilgenberg, Germany), and the measurements on the bulk materials were carried out at 75 °C. The X-ray images were recorded for 900 s with a 2D position sensitive detector (Vantec 2000), corrected for background scattering and radially integrated to obtain the scattering intensity as a function of the scattering vector, $q = (4\pi/\lambda) \sin \theta$, with 2θ being the scattering angle and λ the X-ray wavelength.

Conflict of Interest: The authors declare no competing financial interest.

Acknowledgment. This publication was based on work supported by award no. KUS-C1-018-02, made by King Abdullah University of Science and Technology (KAUST). This material is based upon work supported by the National Science Foundation under Grant No. IIP-1114275 and work supported by NYSERDA under Grant No. 18507. NYSERDA has not reviewed the information contained herein, and the opinions expressed in this report do not necessarily reflect those of NYSERDA or the State of New York. This work made use of the Cornell Center for Materials Research Shared Facilities which are supported through the NSF MRSEC program (DMR-1120296) and of the Nanobiotechnology Center shared research facilities at Cornell. We acknowledge P. Huang, R. Hovden, and J. Mundy of Cornell University for help with the TEM imaging. The Austrian Science Funds FWF (Project No. I449) is acknowledged for financial support.

REFERENCES AND NOTES

1. Kumar, S. K.; Krishnamoorti, R. Nanocomposites: Structure, Phase Behavior, and Properties. *Annu. Rev. Chem. Biomol. Eng.* **2010**, *1*, 37–58.
2. Mackay, M. E.; Tuteja, A.; Duxbury, P. M.; Hawker, C. J.; Horn, B.; Van; Guan, Z.; Chen, G.; Krishnan, R. S. General Strategies for Nanoparticle Dispersion. *Science* **2006**, *311*, 1740–1743.
3. Winey, K. I.; Vaia, R. A. Polymer Nanocomposites. *MRS Bull.* **2011**, *32*, 314–322.
4. Podsiadlo, P.; Kaushik, A. K.; Arruda, E. M.; Waas, A. M.; Shim, B. S.; Xu, J.; Nandivada, H.; Pumplin, B. G.; Lahann, J.; Ramamoorthy, A.; *et al.* Ultrastrong and Stiff Layered Polymer Nanocomposites. *Science* **2007**, *318*, 80–83.
5. Akcora, P.; Kumar, S. K.; Moll, J.; Lewis, S.; Schadler, L. S.; Li, Y.; Benicewicz, B. C.; Sandy, A.; Narayanan, S.; Ilavsky, J.; *et al.* Gel-like Mechanical Reinforcement in Polymer Nanocomposite Melts. *Macromolecules* **2010**, *43*, 1003–1010.
6. Voevodin, A. A; Vaia, R. A; Patton, S. T.; Diamanti, S.; Pender, M.; Yoonessi, M.; Brubaker, J.; Hu, J.-J.; Sanders, J. H.; Phillips, B. S.; *et al.* Nanoparticle-Wetted Surfaces for Relays and Energy Transmission Contacts. *Small* **2007**, *3*, 1957–1963.
7. Kim, D.; Archer, L. A. Nanoscale Organic$-$Inorganic Hybrid Lubricants. *Langmuir* **2011**, *27*, 3083–3094.
8. Bremer, L.; Tuinier, R.; Jahromi, S. High Refractive Index Nanocomposite Fluids for Immersion Lithography. *Langmuir* **2009**, *25*, 2390–2401.
9. Nugent, J. L.; Moganty, S. S.; Archer, L. A. Nanoscale Organic Hybrid Electrolytes. *Adv. Mater.* **2010**, *22*, 3677–3680.
10. Lin, K.-Y. A.; Park, A.-H. A. Effects of Bonding Types and Functional Groups on CO_2 Capture Using Novel Multiphase Systems of Liquid-like Nanoparticle Organic Hybrid Materials. *Environ. Sci. Technol.* **2011**, *45*, 6633–6639.
11. Corbierre, M. K.; Cameron, N. S.; Lennox, R. B. Polymer-Stabilized Gold Nanoparticles with High Grafting Densities. *Langmuir* **2004**, *20*, 2867–2873.
12. Goel, V.; Pietrasik, J.; Dong, H.; Sharma, J.; Matyjaszewski, K.; Krishnamoorti, R. Structure of Polymer Tethered Highly Grafted Nanoparticles. *Macromolecules* **2011**, *44*, 8129–8135.
13. Zhang, Q.; Archer, L. A. Poly(ethylene oxide)/Silica Nanocomposites: Structure and Rheology. *Langmuir* **2002**, *18*, 10435–10442.
14. Ohno, K.; Morinaga, T.; Koh, K.; Tsujii, Y.; Fukuda, T. Synthesis of Monodisperse Silica Particles Coated with Well-Defined, High-Density Polymer Brushes by Surface-Initiated Atom Transfer Radical Polymerization. *Macromolecules* **2005**, *38*, 2137–2142.
15. Ghosh Chaudhuri, R.; Paria, S. Core/Shell Nanoparticles: Classes, Properties, Synthesis Mechanisms, Characterization, and Applications. *Chem. Rev.* **2012**, *112*, 2373–2433.
16. Akcora, P.; Liu, H.; Kumar, S. K.; Moll, J.; Li, Y.; Benicewicz, B. C.; Schadler, L. S.; Acehan, D.; Panagiotopoulos, A. Z.; Pryamitsyn, V.; *et al.* Anisotropic Self-assembly of Spherical Polymer-grafted Nanoparticles. *Nat. Mater.* **2009**, *8*, 354–359.
17. Moganty, S. S.; Jayaprakash, N.; Nugent, J. L.; Shen, J.; Archer, L. A. Ionic-Liquid-Tethered Nanoparticles: Hybrid Electrolytes. *Angew. Chem., Int. Ed.* **2010**, *122*, 9344–9347.

18. Bhattacharjee, R. R.; Li, R.; Estevez, L.; Smilgies, D.-M.; Amassian, A.; Giannelis, E. P. A Plasmonic Fluid with Dynamically Tunable Optical Properties. *J. Mater. Chem.* **2009**, *19*, 8728–8731.
19. Warren, S. C.; Banholzer, M. J.; Slaughter, L. S.; Giannelis, E. P.; DiSalvo, F. J.; Wiesner, U. B. Generalized Route to Metal Nanoparticles with Liquid Behavior. *J. Am. Chem. Soc.* **2006**, *128*, 12074–12075.
20. Sun, L.; Fang, J.; Reed, J. C.; Estevez, L.; Bartnik, A. C.; Hyun, B.-R.; Wise, F. W.; Malliaras, G. G.; Giannelis, E. P. Lead-Salt Quantum-Dot Ionic Liquids. *Small* **2010**, *6*, 638–641.
21. Bourlinos, A. B.; Stassinopoulos, A.; Anglos, D.; Herrera, R.; Anastasiadis, S. H.; Petridis, D.; Giannelis, E. P. Functionalized ZnO Nanoparticles with Liquidlike Behavior and Their Photoluminescence Properties. *Small* **2006**, *2*, 513–516.
22. Bourlinos, A. B.; Giannelis, E. P.; Zhang, Q.; Archer, L. A.; Floudas, G.; Fytas, G. Surface-Functionalized Nanoparticles with Liquid-like Behavior: The Role of the Constituent Components. *Eur. Phys. J. E., Soft Matter* **2006**, *20*, 109–117.
23. Rodriguez, R.; Herrera, R.; Bourlinos, A. B.; Li, R.; Amassian, A.; Archer, L. A.; Giannelis, E. P. The Synthesis and Properties of Nanoscale Ionic Materials. *Appl. Organomet. Chem.* **2010**, *24*, 581–589.
24. Perriman, A. W.; Cölfen, H.; Hughes, R. W.; Barrie, C. L.; Mann, S. Solvent-free Protein Liquids and Liquid Crystals. *Angew. Chem., Int. Ed.* **2009**, *48*, 6242–6246.
25. Fernandes, N.; Dallas, P.; Rodriguez, R.; Bourlinos, A. B.; Georgakilas, V.; Giannelis, E. P. Fullerol Ionic Fluids. *Nanoscale* **2010**, *2*, 1653–1656.
26. Bourlinos, A. B.; Herrera, R.; Chalkias, N.; Jiang, D. D.; Zhang, Q.; Archer, L. A.; Giannelis, E. P. Surface-Functionalized Nanoparticles with Liquid-like Behavior. *Adv. Mater.* **2005**, *17*, 234–237.
27. Bourlinos, A. B.; Ray Chowdhury, S.; Herrera, R.; Jiang, D. D.; Zhang, Q.; Archer, L. A.; Giannelis, E. P. Functionalized Nanostructures with Liquid-Like Behavior: Expanding the Gallery of Available Nanostructures. *Adv. Funct. Mater.* **2005**, *15*, 1285–1290.
28. Koning, C.; Duin, M. Van; Pagnoulle, C.; Jerome, R. Strategies for Compatibilization of Polymer Blends. *Prog. Polym. Sci.* **1998**, *23*, 707–757.
29. Wang, Z.-G. Chain Dimensions in Amorphous Polymer Melts. *Macromolecules* **1995**, *28*, 570–576.
30. Allen, L. H.; Matijevic, E. Stability of Colloidal Silica. *J. Colloid Interface Sci.* **1970**, *33*, 420–429.
31. Allen, L. H.; Matijevic, E.; Meites, L. Exchange of Na^+ for the Silanolic Protons of Silica. *J. Inorg. Nucl. Chem.* **1971**, *33*, 1293–1299.
32. Iler, R. K. *The Chemistry of Silica*; John Wiley & Sons, Inc.: New York, 1979; p 865.
33. Leung, K.; Nielsen, I. M. B.; Criscenti, L. J. Elucidating the Bimodal Acid-base Behavior of the Water–Silica Interface from First Principles. *J. Am. Chem. Soc.* **2009**, *131*, 18358–18365.
34. Rosenholm, J. M.; Czuryszkiewicz, T.; Kleitz, F.; Rosenholm, J. B.; Lindén, M. On the Nature of the Brønsted Acidic Groups on Native and Functionalized Mesoporous Siliceous SBA-15 as Studied by Benzylamine Adsorption from Solution. *Langmuir* **2007**, *23*, 4315–4323.
35. Madathingal, R. R.; Wunder, S. L. Confinement Effects of Silica Nanoparticles with Radii Smaller and Larger Than R_g of Adsorbed Poly(ethylene oxide). *Macromolecules* **2011**, *44*, 2873–2882.
36. Mathur, S.; Moudgil, B. Adsorption Mechanism(s) of Poly-(ethylene oxide) on Oxide Surfaces. *J. Colloid Interface Sci.* **1997**, *196*, 92–98.
37. Brunner-Popela, J.; Mittelbach, R.; Strey, R.; Schubert, K.-V.; Kaler, E. W.; Glatter, O. Small-Angle Scattering of Interacting Particles. III. $D_2O-C_{12}E_5$ Mixtures and Microemulsions with *n*-Octane. *J. Chem. Phys.* **1999**, *110*, 10623–10632.
38. Freltoft, T.; Kjems, J.; Sinha, S. Power-Law Correlations and Finite-Size Effects in Silica Particle Aggregates Studied by Small-Angle Neutron Scattering. *Phys. Rev. B* **1986**, *33*, 269–275.
39. Teixeira, J. Small-Angle Scattering by Fractal Systems. *J. Appl. Crystallogr.* **1988**, *21*, 781–785.
40. Brunner-Popela, J.; Glatter, O. Small-Angle Scattering of Interacting Particles. I. Basic Principles of a Global Evaluation Technique. *J. Appl. Crystallogr.* **1997**, *30*, 431–442.
41. Weyerich, B.; Brunner-Popela, J.; Glatter, O. Small-Angle Scattering of Interacting Particles. II. Generalized Indirect Fourier Transformation under Consideration of the Effective Structure Factor for Polydisperse Systems. *J. Appl. Crystallogr.* **1999**, *32*, 197–209.
42. Hayter, J. B.; Penfold, J. An Analytic Structure Factor for Macroion Solutions. *Mol. Phys.* **1981**, *42*, 109–118.
43. Hansen, J.-P.; Hayter, J. B. A Rescaled MSA Structure Factor for Dilute Charged Colloidal Dispersions. *Mol. Phys.* **1982**, *46*, 651–656.
44. Srivastava, S.; Shin, J. H.; Archer, L. A. Structure and Rheology of Nanoparticle–Polymer Suspensions. *Soft Matter* **2012**, *8*, 4097–4108.
45. Dukes, D.; Li, Y.; Lewis, S.; Benicewicz, B. C.; Schadler, L.; Kumar, S. K. Conformational Transitions of Spherical Polymer Brushes: Synthesis, Characterization, and Theory. *Macromolecules* **2010**, *43*, 1564–1570.
46. Yu, H.-Y.; Koch, D. L. Structure of Solvent-Free Nanoparticle-Organic Hybrid Materials. *Langmuir* **2010**, *26*, 16801–16811.
47. Goel, V.; Pietrasik, J.; Matyjaszewski, K.; Krishnamoorti, R. Linear Viscoelasticity of Spherical SiO_2 Nanoparticle-Tethered Poly(butyl acrylate) Hybrids. *Ind. Eng. Chem. Res.* **2010**, *49*, 11985–11990.
48. Jespersen, M. L.; Mirau, P. A.; Meerwall, E.; von; Vaia, R. A.; Rodriguez, R.; Giannelis, E. P. Canopy Dynamics in Nanoscale Ionic Materials. *ACS Nano* **2010**, *4*, 3735–3742.
49. Chremos, A.; Panagiotopoulos, A. Z.; Koch, D. L. Dynamics of Solvent-free Grafted Nanoparticles. *J. Chem. Phys.* **2012**, *136*, 044902–1–044902–9.
50. Goyal, S.; Escobedo, F. A Structure and Transport Properties of Polymer Grafted Nanoparticles. *J. Chem. Phys.* **2011**, *135*, 184902–1–184902–12.